Leucyl-tRNA Synthetase Deficiency Systemically Induces Excessive Autophagy in Zebrafish

Hiroshi Shiraishi
Oita University
Nobuyuki Shimizu
Oita University
Mika Tsumori
Oita University
Kyoko Kiyota
Oita University
Miwako Maeda
Oita University
Tohru Ishitani
Osaka University
Reiko Hanada
Oita University
Kenji Ihara
Oita University
Toshikatsu Hanada (thanada@oita-u.ac.jp)
Oita University
Masanori Inoue
Oita University
Hiroaki Miyahara
Aichi Medical University

Research Article

Keywords: LARS, liver, Aminoacyl

Posted Date: January 5th, 2021

DOI: https://doi.org/10.21203/rs.3.rs-132893/v1

Version of Record: A version of this preprint was published at Scientific Reports on April 16th, 2021. See the published version at https://doi.org/10.1038/s41598-021-87879-4.

Leucyl-tRNA synthetase deficiency systemically induces excessive autophagy in zebrafish

Masanori Inoue[a, b], Hiroaki Miyahara[c], Hiroshi Shiraishi[a], Nobuyuki Shimizu[a], Mika Tsumori[b], Kyoko Kiyota[b], Miwako Maeda[b], Tohru Ishitani[d], Reiko Hanada[e], Kenji Ihara[b,*] & Toshikatsu Hanada[a,*]

[a]Department of Cell Biology, Oita University Faculty of Medicine, Yufu, Oita 879-5593, Japan

[b]Department of Pediatrics, Oita University Faculty of Medicine, Yufu, Oita 879-5593, Japan

[c]Department of Neuropathology, Institute for Medical Science of Aging, Aichi Medical University, Aichi 480-1195, Japan

[d]Department of Homeostatic Regulation, Division of Cellular and Molecular Biology, Research Institute for Microbial Diseases, Osaka University, Osaka 565-0871, Japan

[e]Department of Neurophysiology, Oita University Faculty of Medicine, Yufu, Oita 879-5593, Japan

***Corresponding author**

Correspondence and requests for materials should be addressed to Kenji Ihara or Toshikatsu Hanada

Department of Cell Biology, Oita University Faculty of Medicine, Yufu, Oita 879-5593, Japan

Tel.: +81-97-586-5662; Fax: +81-97-586-5665;

E-mail: k-ihara@oita-u.ac.jp; thanada@oita-u.ac.jp

Abstract

Leucyl-tRNA synthetase (LARS) is an enzyme that catalyses the ligation of leucine with leucine tRNA. LARS is also essential to sensitize the intracellular leucine concentration to the mammalian target of rapamycin complex 1 (mTORC1) activation. Biallelic mutation in the *LARS* gene causes infantile liver failure syndrome type 1 (ILFS1), which is characterized by acute liver failure, anaemia, and neurological disorders, including microcephaly and seizures. However, the molecular mechanism underlying ILFS1 under LARS deficiency has been elusive. Here, we generated Lars deficient (*larsb*$^{-/-}$) zebrafish that showed progressive liver failure and anaemia, resulting in early lethality within 12 days post fertilization. The *atg5*-morpholino knockdown and bafilomycin treatment partially improved the size of the liver and survival rate in *larsb*$^{-/-}$ zebrafish. These findings indicate the involvement of autophagy in the pathogenesis of *larsb*$^{-/-}$ zebrafish. Indeed, excessive autophagy activation was observed in *larsb*$^{-/-}$ zebrafish. Therefore, our data clarify a mechanistic link between LARS and autophagy *in vivo*. Furthermore, autophagy regulation by LARS could lead to development of new therapeutics for IFLS1.

Introduction

Aminoacyl-tRNA synthetases (ARSs) are essential enzymes that catalyse the ligation of amino acids to their cognate transfer RNAs (tRNAs), which is the first step in protein synthesis[1-4]. Leucyl-tRNA synthetase (LARS), a component of the multi-tRNA synthetase complex, is critical for charging leucine tRNA with leucine[3]. Furthermore, LARS has a non-canonical role as a mammalian target of rapamycin complex 1 (mTORC1)-associated protein required for amino acid-induced mTORC1 activation, indicating that LARS is not only a tRNA synthetase, but also an intracellular leucine sensor for mTORC1 signalling[5-8].

The alternative functions of ARSs play a critical role in cellular homeostasis, including translation control, transcription regulation, cell migration, inflammatory responses, tumorigenesis, and cell death regulation[9,10]. These functions may explain the mechanisms of several human diseases caused by ARS gene mutations, including cancer, neurological disorders, and autoimmune diseases[4,11-14]. Biallelic mutation in the cytoplasmic *LARS* leads to an infantile hepatopathy called infantile liver failure syndrome type 1 (ILFS1), which is characterized by acute liver failure in the first few months and is associated with failure to thrive, anaemia, microcephaly, muscular hypotonia, and seizures[15,16].

Although LARS is involved in mTORC1 pathways and its dysfunction may be responsible for ILFS1 pathology, the function of LARS *in vivo* has remained elusive. Previous research using a Lars loss of function (*larsb*$^{-/-}$) zebrafish model revealed that the mutant zebrafish exhibit a phenotype similar to that of ILFS1[17]. Moreover, in contrast to a previous study showing that ablation of LARS desensitizes the mTORC1 pathway to amino acids in yeast and human cell lines[5,6], the *larsb*$^{-/-}$ zebrafish shows augmented mTORC1 activation[17]. Furthermore, suppression of mTORC1 activation by rapamycin treatment or knockdown of mTORC1 by morpholino partially rescues the phenotype of *larsb*$^{-/-}$ zebrafish[17].

Therefore, to gain further insight into the LARS-mTORC1-autophagy circuit, we examined the involvement of autophagy in the pathogenesis of *larsb*$^{-/-}$ zebrafish.

Results

Generation of larsb$^{-/-}$ *zebrafish*

To assess the function of LARS *in vivo*, we generated larsb-knockout (*larsb*$^{-/-}$) zebrafish using CRISPR/Cas9 technology[18,19]. Two genes, *larsa* and *larsb* encode cytosolic Lars in zebrafish, and among them, *larsb* shares higher homology with human *LARS*.

To obtain *larsb* mutant zebrafish, we designed the CRISPR/Cas9 target site in exon 3 of *larsb* (Fig. 1A), which corresponds to the editing domain of the Lars protein (Fig. 1B). Notably, most *LARS* gene mutations in humans occur in the editing domain[15,16,20], indicating that this domain has an essential function *in vivo*. After screening several founders that transmitted targeted indels to the F1 progeny, we established a stable line with a frameshift mutation caused by a 5-bp deletion (Fig. 1A). Western blotting confirmed a complete lack of the Lars protein in *larsb*$^{-/-}$ larvae (Fig. 1B).

Liver defects and early lethality in larsb$^{-/-}$ zebrafish

Larsb $^{-/-}$ larvae had hatching rates and timings comparable with that of *larsb*$^{+/+}$ larvae. However, all *larsb*$^{-/-}$ larvae exhibited thinness, cardiac edema, and swim bladder deflation (Fig. 2A). All *larsb*$^{-/-}$ larvae died between 8 and 11 days post fertilization (dpf) (Fig. 2B). Because anaemia is one of the typical symptoms in ILFS1 patients, we performed o-dianisidine staining to detect haemoglobin-containing cells in *larsb*$^{-/-}$ larvae. As expected, the *larsb*$^{-/-}$ larvae showed anaemia (Fig. 2C)[15].

We further analysed the morphological changes in liver development by crossing *larsb*$^{-/-}$ zebrafish with Tg[*fabp10:*mcherry] transgenic zebrafish, which express mCherry fluorescent protein specifically in the liver[21,22]. The livers of *larsb*$^{-/-}$ larvae were significantly smaller than that of *larsb*$^{+/+}$ larvae at 3 dpf, and showed no further

development until their death ($P < 0.001$; Figs. 2D and E). These data indicate the similarity of *larsb*$^{-/-}$ zebrafish phenotype to ILFS1 due to human *LARS* mutation. Thus, the *in vivo* function of LARS seems to be conserved across zebrafish and humans.

Lars deficiency induces autophagy in larsb*$^{-/-}$ *zebrafish

To assess liver abnormalities in *larsb*$^{-/-}$ zebrafish, we performed histopathological examination. The livers of *larsb*$^{-/-}$ larvae drastically reduced in size compared with that of *larsb*$^{+/+}$ larvae (Fig. 3A). In addition, large vacuolations, which seemed to disappear in the cytoplasm, were observed in the livers of *larsb*$^{-/-}$ larvae. Some large vacuolations included a bare nucleus. These findings indicate autophagic cell death[23]. Indeed, microtubule-associated protein 1A/1B-light chain 3 (LC3B)-II, a standard marker of autophagosome formation, was upregulated in *larsb*$^{-/-}$ larvae (Fig. 3B), as shown by western blotting. The selective autophagy substrate p62 was also more degraded in *larsb*$^{-/-}$ larvae than in *larsb*$^{+/+}$ larvae (Fig. 3B). However, histologically, cytoplasmic condensation, cytoplasmic blebbing, and fragmented nuclei, which indicate apoptotic cell death, were not observed in the livers of *larsb*$^{-/-}$ larvae. These results indicate that apoptotic cell death is not induced by Lars deficiency.

Next, to examine whether autophagy is involved in liver abnormalities, we evaluated the status of autophagy by fluorescent immunostaining for Lc3b in *larsb*$^{-/-}$ larvae under

Tg[*fabp10*:mcherry] background. Lc3b, a downstream constituent of the autophagy pathway and participant in autophagosome formation, is widely used to monitor autophagy[24]. Although *larsb*$^{+/+}$ larvae had no apparent autophagic structures in the liver, *larsb*$^{-/-}$ larvae displayed large vacuoles, including floating nuclei and various sized dots with Lc3b immunoreactivity, thereby indicating autophagic cell death (Fig. 3C). Hepatocellular nucleophagy, showing fragmented nuclei labelled with Lc3b, was also observed in the livers of *larsb*$^{-/-}$ larvae. Moreover, many autophagosomal structures visualized with Lc3b were also observed in the skeletal muscles and spinal cords of *larsb*$^{-/-}$ larvae in comparison to *larsb*$^{+/+}$ larvae. Thus, these data indicate that Lars deficiency induces autophagy not only in the liver, but also in the central nervous system and skeletal muscle during the early embryonic stage.

Immunoelectron microscopy analysis of larsb$^{-/-}$ larvae

We next assessed the ultrastructure of the liver, skeletal muscle, and spinal cord by immunoelectron microscopy. There were no overt autophagic structures in the livers, skeletal muscles, and spinal cords of *larsb*$^{+/+}$ larvae (Figs. 4A-C). However, large vacuoles in the livers of *larsb*$^{-/-}$ larvae were composed of numerous irregular membranous structures with immunoreactivity against both Lc3b and red fluorescent protein (RFP) (Figs. 4D and G). Many irregular structures labelled with anti-Lc3b antibody, which were

presumed to be autophagosomes or autolysosomes, were also observed in the muscles and spinal cords of *larsb*$^{-/-}$ larvae compared with those of *larsb*$^{+/+}$ larvae (Figs. 4E, F, H, and I). Therefore, although autophagy caused by Larsb deficiency occurred in some tissues, including the skeletal muscle and spinal cord, the liver was the most damaged tissue in *larsb*$^{-/-}$ zebrafish.

Inhibition of autophagy partially rescues the liver defects

To verify whether the liver defects and severe developmental abnormalities in *larsb*$^{-/-}$ larvae were due to autophagy, we performed a knockdown experiment using an antisense morpholino for *atg5* (atg5-MO), which is essential for autophagy induction[25]. As a highly efficient *atg5* knockdown in zebrafish causes abnormal neuronal development[26], the amount of MO injected was estimated to achieve a knockdown efficiency of 60% (Supplementary Figs. S1A and B). As expected, atg5-MO prevented abnormal embryonic development, such as cardiac edema and swim-bladder deflation in *larsb*$^{-/-}$ larvae (Fig. 5A). Atg5-MO also partially rescued the liver defects in *larsb*$^{-/-}$ larvae (Figs. 5B and C). However, atg5-MO did not improve the survival rate of *larsb*$^{-/-}$ zebrafish, presumably because of its transient effectiveness for up to 5 days after injection (Supplementary Fig. S2).

To validate whether autophagy is involved in the *larsb*$^{-/-}$ phenotype, we treated *larsb*$^{-/-}$ larvae with the specific autophagy inhibitor bafilomycin[27]. Bafilomycin treatment partially improved the size of the liver in *larsb*$^{-/-}$ larvae (Figs. 5D and E). Notably, we observed a significant improvement in cardiac edema after treating *larsb*$^{-/-}$ larvae with bafilomycin (Fig. 5D). The survival rate was also significantly enhanced by bafilomycin treatment (Fig. 5F). In contrast, the mTORC1 inhibitor rapamycin had no effect on the survival of *larsb*$^{-/-}$ larvae (Supplementary Fig. S3). These experiments provide direct evidence that hyperactivated autophagy induced by Lars deficiency is responsible for the liver defects and an early lethality.

Discussion

In this study, we provide evidence on the *in vivo* function of LARS in autophagy regulation. *Larsb*$^{-/-}$ zebrafish displayed liver failure and anaemia, a phenotype similar to ILFS1 caused by human *LARS* gene mutations. Histopathological analysis of *larsb*$^{-/-}$ zebrafish showed enhanced autophagy not only in the liver, but also in other tissues, including the nervous system and muscles, during early embryonic development. In addition, huge vacuolations with bare nuclei were observed in the livers of *larsb*$^{-/-}$ zebrafish, indicating severe autophagic cell death. Inactivation of autophagy by *atg5*

knockdown or bafilomycin treatment partially rescued early lethality with liver failure. These results imply that the loss-of-function mutations of *LARS* in ILFS1 cause severe autophagic cell death in the liver.

Previously, *in vitro* studies have shown that LARS induces mTORC1 activation by sensing abundant intracellular leucine concentration, thereby inhibiting autophagy[5,6]. In contrast, LARS dysfunction activates autophagy by inhibiting mTORC1 activity[5,6]. These findings indicate the essential function of LARS in regulating autophagy. Wang et al. through *in vivo* studies have shown that *larsb*$^{-/-}$ zebrafish have severe liver failure and increased mTORC1 activation[17]. Rapamycin, an mTORC1 inhibitor, partially rescues liver failure in *larsb*$^{-/-}$ zebrafish, suggesting that hyperactivation of mTORC1 may be related to the onset of ILFS1[17]. Therefore, there seems to be a discrepancy between the *in vitro* and *in vivo* experiments.

Our histopathological data clearly showed that *larsb*$^{-/-}$ zebrafish had increased autophagy in several tissues, including the skeletal muscle and central nervous system as well as the liver. Systemic autophagy induced by Lars deficiency could explain the general symptoms of ILFS1, such as muscle hypotonia, mental retardation, and convulsions[15,16]. Notably, Lars deficiency-induced autophagy caused significant damage to the liver. In the muscle tissue, the mTORC1-dependent autophagy pathway is mainly

regulated by insulin signalling, whereas in the liver, it is strongly regulated by amino acid concentrations[28]. As LARS is a leucine concentration sensor for amino acid signalling to mTORC1, LARS may play an essential role in autophagy regulation, especially in the liver.

Our experiments suggest a mechanistic link between ILFS1 and *LARS* loss-of-function mutations. Although rapamycin had no effect on the phenotype of *larsb*$^{-/-}$ larvae, *atg5* knockdown and the lysosome-degrading enzyme inhibitor bafilomycin A1 partially improved the survival rate and liver damage. Therefore, suppression of excessive autophagy may rescue the symptoms of ILFS1. Of note, *larsb*$^{-/-}$ zebrafish exhibited a more severe phenotype than ILFS1, although the phenotype closely resembled the symptoms of ILFS1. The exact molecular mechanism by which *LARS* mutation influences human ILFS1 needs to be determined using knock-in animal models, wherein a corresponding mutation is introduced into the zebrafish *larsb* locus. Moreover, there is increasing evidence for autophagy being associated with many diseases, including sepsis, Parkinson's disease, and Alzheimer's disease[29-31]. Hence, autophagy regulation by *LARS* may lead to new therapeutics for these related disorders.

Methods

Zebrafish maintenance

Zebrafish AB genetic background *larsb* mutant and Tg[*fabp10*:mcherry][21,22] were raised and maintained following standard procedures. They were kept at 28–29 °C under a 14-h:10-h light:dark cycle. Embryos were collected and housed at 28.5 °C. All animal experimental procedures were performed in accordance with the institutional and national guidelines and regulations. The study was carried out in compliance with the ARRIVE guidelines. The study protocol was approved by the Institutional Review Board of Oita University (approval no. 180506).

Generation of the larsb$^{-/-}$ zebrafish line

A *larsb*$^{-/-}$ zebrafish line was generated via CRISPR/ Cas9 gene editing[18,19]. The site of the *larsb* sgRNA target was 5'-CAGTGTGCCGTCAGATGCACCGG-3', in the editing domain of the LARS protein. Cas9 protein (300 pg) and gRNA (30 pg) were injected into one-cell-stage wild-type embryos. The mutation at the target site was verified via Sanger sequencing. The injected embryos were raised until adulthood and outcrossed with wild-type adults. DNA extracted from the F1 generation of whole larvae at 24 h post fertilization (hpf) was screened for indels by the heteroduplex mobility assay[32,33] and Sanger sequencing. The F0 founder with germline transmission was selected to establish the knockout zebrafish line. F1 generations were raised to adulthood, had their fins

clipped, and were sequenced. Fish carrying the same mutation (deletion of CACCG) were identified. All experiments were performed on embryos from the F2 or F3 progeny.

Generation of transgenic zebrafish

Tg[*fabp10*:mCherry] fish expressing mCherry exclusively in hepatocytes were generated using MultiSite Gateway™ kit (Thermo Fisher Scientific, Waltham, MA, USA) to produce vectors with Tol2 transposon sites[34]. A 2.8-kb promoter of the *fabp10* gene[21] was cloned into the p5E-mcs vector. Multisite Gateway cloning[35] was performed with the destination vector pDestTol2pA2, the 5' entry vector containing the fabp10 promoter, the middle entry vector containing pME-mCherry, and the 3' entry vector containing p3E-polyA. DNA constructs (25 pg) and Tol2 mRNA (25 pg) were injected into wild-type zebrafish embryos at the one-cell stage.

Western blotting

Western blotting was performed with antibodies against Lars (Cell Signaling Technology, Beverly, MA, USA), p62 (Medical & Biological Laboratories, Nagoya, Japan), LC3B (Medical & Biological Laboratories), ATG5 (Novus Biologicals, Littleton, CO, USA), β-actin (Sigma-Aldrich, St. Louis, MO, USA), and glyceraldehyde 3-phosphate dehydrogenase (GAPDH) (Sigma-Aldrich). Samples for western blotting were lysed with lysis buffer (0.5% NP-40, 10% glycerin, 50 mM HEPES-KOH (pH 7.8), 150 mM NaCl,

and 1 mM EDTA) with protease and phosphatase inhibitor cocktail (Thermo Fisher Scientific). Total proteins were separated by SDS-PAGE, transferred to Immobilon-P membranes (Millipore, Billerica, MA, USA), and probed with the above-mentioned antibodies.

O-dianisidine staining

The embryos at 72 hpf were incubated in o-dianisidine staining buffer (0.6 mg/mL o-dianisidine, 10 mM sodium acetate, 0.65% hydrogen peroxide, and 40% ethanol) for 15 min in the dark.

Morphological analyses

Zebrafish larvae were placed in 3% methylcellulose, and images were acquired using a Leica M205 FA fluorescent stereo microscope. The liver size was measured manually using Image J software.

Zebrafish survival analysis

Embryos were generated and housed at 28.5 °C. Larvae were transferred to rotifer feeding solution at 5 dpf, and the solution was replaced daily with additional rotifer feeding solution. The dishes were monitored twice a day until 12 dpf.

Histopathological staining and fluorescent immunostaining

Small larvae specimens were fixed with 0.1% glutaraldehyde in 4% paraformaldehyde

for approximately 48 h, and washed with phosphate-buffered saline. Then, the specimens were washed with gradually increasing concentrations of dimethylformamide and embedded in LR White resin (London Resin Company, Berkshire, UK). Histological examinations were performed using semi-thin sections (1 μm thick) and stained with toluidine blue dye. A double-labelling immunofluorescence analysis was performed on the semi-thin sections using the following primary antibodies: rabbit polyclonal LC3B antibody (Abcam, Cambridge, UK; 1:100), and mouse monoclonal RFP antibody (clone GA5; Chemicon; 1:100). The secondary antibodies used were Alexa Fluor 488 goat anti-rabbit IgG (Molecular Probes, Eugene, OR, USA; 1:500) and Alexa Fluor 568 goat anti-mouse IgG (Molecular Probes; 1:500). Vectashield DAPI (Vector Laboratories, Brussels, Belgium) was used as a nuclear marker. A laser scanning confocal microscope (BZ-X800, Keyence, Osaka, Japan) equipped with a ×100 oil immersion objective was used to visualize immunoreactivity.

Immunoelectron microscopy

The ultrastructural localization of LC3B was examined using zebrafish larvae, employing the post-embedding method as described previously[36,37]. Small larvae specimens embedded in LR White Resin, prepared as semi-thin sections, were used. Ultra-thin sections (70 nm thick) were cut, incubated with a rabbit polyclonal LC3B antibody

(1:300) and a mouse monoclonal RFP antibody (1:100) for 2 h at 24 °C , and reacted with 10-nm gold colloidal particle-conjugated anti-rabbit IgG (British BioCell International, Cardiff, UK; 1:30) and 5-nm gold colloidal particle-conjugated anti-mouse IgG (British BioCell International; 1:30). Finally, the sections were stained with lead citrate and examined using a JEM-1400 electron microscope at 80 kV (JEOL, Tokyo, Japan).

Morpholino oligonucleotide injection

Morpholino oligonucleotide for *atg5* (5'-CATCCTTGTCATCTGCCATTATCAT-3') was obtained from Gene-Tools, LLC (Philomath, OR, USA). The *atg5* morpholino oligo was used to inhibit *atg5* translation by binding to *atg5* initiation sites[26]. *Atg5* morpholino oligo or control morpholino oligo (0.02 pmol) was injected into the zebrafish eggs at the one-cell stage.

Bafilomycin and rapamycin treatments

Embryos were treated with bafilomycin A1 (2.5 nM; EMD Millipore, Darmstadt, Germany), rapamycin (5 μM; LC Laboratories, Woburn, MA, USA), or dimethyl sulfoxide (DMSO) as the control, in egg water from 48 hpf to 72 hpf for morphological experiments and in the larval stage from 4 dpf to 13 dpf for survival experiments. The water containing the drug was replaced daily.

Statistics

Statistical analyses were performed using GraphPad Prism (GraphPad Software, Inc., San Diego, CA, USA). All values are expressed as mean ± SEM. Comparisons between groups were made by Student's t-test. Statistical difference for survival curves were analysed using a Log-rank (Mantel-Cox) test. $P < 0.05$ was considered statistically significant.

Acknowledgments

We thank M. Nakamura-Ota, K. Shimizu, and M. Iwao for their excellent technical assistance. TH was supported by the Japan Society for the Promotion of Science [20H03644], the Takeda Science Foundation, the Kamizono Kids Clinic, and the Mizoguchi Urology Clinic. MI was supported by the Japan Society for the Promotion of Science [19K17366].

Author contributions

MI generated mutant zebrafish and performed zebrafish phenotyping with the assistance of MT, KK, and MM. HM performed the histological analysis. HS and NS performed the biochemical assays. TI and RH provided key reagents and technical assistance for the generation of mutant zebrafish. KI and TH coordinated the project and wrote the

manuscript. All authors reviewed the manuscript.

Competing interests

The authors declare no competing interests.

Figure legends

Figure 1. Construction of *larsb*-knockout mutant zebrafish line.

(A) Diagram showing the *larsb* genomic locus, CRISPR/Cas9 target site, and *larsb*-knockout (*larsb*$^{-/-}$) zebrafish mutant genotype. The sgRNA target sequence is displayed in green and the PAM region in red. In the genomic sequencing analysis chromatograms, the deletion region in the mutant *larsb*$^{-/-}$ zebrafish is shown by the red box. (B) The Lars protein of *larsb*$^{-/-}$ zebrafish had a missing editing domain. Western blotting analysis of the Lars protein expression in *larsb*$^{+/+}$ and *larsb*$^{-/-}$ zebrafish. β-actin levels served as the loading control. Lars: leucyl-tRNA synthetase.

Figure 2. *Larsb*-knockout larvae display severe developmental phenotype and liver abnormality with early lethality.

(A) Bright field lateral views of *larsb*$^{+/+}$ and *larsb*$^{-/-}$ embryos at 96 h post fertilization (hpf). Scale bar: 500 μm (top row) and 300 μm (bottom row). (B) Kaplan–Meier survival curve of *larsb*$^{+/+}$ (n = 32), *larsb*$^{+/-}$ (n = 63), and *larsb*$^{-/-}$ (n = 23) larvae. (C) Lateral views of *larsb*$^{+/+}$ and *larsb*$^{-/-}$ embryos containing haemoglobin-containing cells (white arrows) stained with o-dianisidine at 72 hpf. (D) Morphological abnormality at 3 dpf and 6 dpf in the livers of *larsb*$^{-/-}$ larvae under Tg[*fabp10*:mcherry] background. Scale bar: 300 μm. (E) Quantification of liver size in larsb$^{-/-}$ larvae under Tg[*fabp10*:mcherry] background (3 dpf

and 6 dpf). n = 5 fish/group. Error bars indicate SEM. Student's t-test; ***P < 0.001. Lars: leucyl-tRNA synthetase; dpf: days post fertilization.

Figure 3. Histopathology and fluorescent immunostaining of *larsb*-knockout larvae.

(A) Lower magnification sagittal views (top row) and higher magnification views (bottom row) of *larsb*$^{+/+}$ and *larsb*$^{-/-}$ larvae. Huge vacuolations, which seemed to disappear in the cytoplasm, were seen in the livers of *larsb*$^{-/-}$ larvae (black arrows), and some large vacuolations included a bare nucleus (black arrowheads). Scale bar: 25 μm. (B) Western blotting analysis of p62 and LC3B protein expression in *larsb*$^{+/+}$ and *larsb*$^{-/-}$ larvae. β-actin levels served as the loading control. (C) Lower magnification sagittal views of *larsb*$^{+/+}$ and *larsb*$^{-/-}$ larvae (top row). Fluorescent immunostaining against LC3B (green) and DAPI (blue) of the livers, skeletal muscles, and spinal cords of *larsb*$^{+/+}$ and *larsb*$^{-/-}$ larvae. Livers of *larsb*$^{-/-}$ larvae had large vacuoles, including floating nuclei and various sized dots with LC3B immunoreactivity (white arrows). Skeletal muscles and spinal cords of *larsb*$^{-/-}$ larvae had many dots with LC3B immunoreactivity (white arrowheads). Scale bar: 10 μm. Lars: leucyl-tRNA synthetase; LC3B: microtubule-associated protein 1A/1B-light chain 3; DAPI: 4′,6-diamidino-2-phenylindole.

Figure 4. Immunoelectron microscopy of *larsb*-knockout larvae.

(A-C) Immunoelectron microscopy of the liver, skeletal muscle, and spinal cord of

larsb$^{+/+}$ larva. (D-I) Immunoelectron microscopy of the liver, skeletal muscle, and spinal cord of *larsb*$^{-/-}$ larva. The bottom row shows higher magnification images (G-I). Large vacuoles in the livers of *larsb*$^{-/-}$ larvae (asterisks) were composed of numerous irregular membranous structures, which showed immunoreactivity against both Lc3b (black arrows) and RFP (black arrowheads) (D and G). Scale bar: 5.0 μm for A and D; 1.0 μm for B and E; 500 nm for C, F, and H; 100 nm for G and I. AP: autophagosome, N: nucleus; Lars: leucyl-tRNA synthetase; Lc3b: microtubule-associated protein 1A/1B-light chain 3; RFP: red fluorescent protein.

Figure 5. Inhibition of autophagy prevents abnormal development and improves survival in *larsb*-knockout larvae.

(A) Morphology of *larsb*$^{+/+}$ and *larsb*$^{-/-}$ embryos injected with either control MO or atg5-MO (72 h post fertilization (hpf)). Scale bars: 500 μm. (B) Morphological abnormality at 72 hpf in the livers of *larsb*$^{-/-}$ larvae under Tg[*fabp10*:mcherry] background injected with either control MO or atg5-MO. Scale bars: 200 μm. (C) Quantification of liver size in *larsb*$^{-/-}$ larvae under Tg[*fabp10*:mcherry] background (72 hpf); n = 4 fish/group. Error bars indicate SEM. Student's t-test; ***P < 0.001. (D) Morphological abnormality at 72 hpf in the livers of *larsb*$^{-/-}$ larvae under Tg[*fabp10*:mcherry] background treated with DMSO or bafilomycin. Scale bars: 200 μm. (E) Quantification of liver size in *larsb*$^{-/-}$

larvae under Tg[*fabp10*:mcherry] background (72 hpf); n = 10 fish/group. Error bars indicate SEM. Student's t-test; *P < 0.05. (F) Kaplan–Meier survival curve of *larsb*$^{+/+}$ (n = 23) and *larsb*$^{-/-}$ (n = 15) larvae treated with DMSO, and *larsb*$^{+/+}$ (n = 11) and *larsb*$^{-/-}$ larvae (n = 21) treated with bafilomycin. Lars: leucyl-tRNA synthetase; MO: morpholino; n.s.: non-significant; DMSO: dimethyl sulfoxide; Dpf: days post fertilization.

References

1 Schimmel, P. Aminoacyl tRNA synthetases: general scheme of structure-function relationships in the polypeptides and recognition of transfer RNAs. *Annu Rev Biochem* **56**, 125-158, doi:10.1146/annurev.bi.56.070187.001013 (1987).

2 Antonellis, A. & Green, E. D. The role of aminoacyl-tRNA synthetases in genetic diseases. *Annu Rev Genomics Hum Genet* **9**, 87-107, doi:10.1146/annurev.genom.9.081307.164204 (2008).

3 Yao, P. & Fox, P. L. Aminoacyl-tRNA synthetases in medicine and disease. *EMBO Mol Med* **5**, 332-343, doi:10.1002/emmm.201100626 (2013).

4 Meyer-Schuman, R. & Antonellis, A. Emerging mechanisms of aminoacyl-tRNA synthetase mutations in recessive and dominant human disease. *Hum Mol Genet* **26**, R114-R127, doi:10.1093/hmg/ddx231 (2017).

5 Han, J. M. *et al.* Leucyl-tRNA synthetase is an intracellular leucine sensor for the mTORC1-signaling pathway. *Cell* **149**, 410-424, doi:10.1016/j.cell.2012.02.044 (2012).

6 Bonfils, G. *et al.* Leucyl-tRNA synthetase controls TORC1 via the EGO complex. *Mol Cell* **46**, 105-110, doi:10.1016/j.molcel.2012.02.009 (2012).

7 He, C. & Klionsky, D. J. Regulation mechanisms and signaling pathways of autophagy. *Annu Rev Genet* **43**, 67-93, doi:10.1146/annurev-genet-102808-114910 (2009).

8 Kim, J. H. *et al.* Control of leucine-dependent mTORC1 pathway through chemical intervention of leucyl-tRNA synthetase and RagD interaction. *Nat Commun* **8**, 732, doi:10.1038/s41467-017-00785-0 (2017).

9 Park, S. G., Ewalt, K. L. & Kim, S. Functional expansion of aminoacyl-tRNA synthetases and their interacting factors: new perspectives on housekeepers. *Trends Biochem Sci* **30**, 569-574, doi:10.1016/j.tibs.2005.08.004 (2005).

10 Guo, M. & Schimmel, P. Essential nontranslational functions of tRNA synthetases. *Nat Chem Biol* **9**, 145-153, doi:10.1038/nchembio.1158 (2013).

11 van Meel, E. *et al.* Rare recessive loss-of-function methionyl-tRNA synthetase mutations presenting as a multi-organ phenotype. *BMC Med Genet* **14**, 106, doi:10.1186/1471-2350-14-106 (2013).

12 Kopajtich, R. *et al.* Biallelic IARS Mutations Cause Growth Retardation with Prenatal Onset, Intellectual Disability, Muscular Hypotonia, and Infantile Hepatopathy. *Am J Hum Genet* **99**, 414-422, doi:10.1016/j.ajhg.2016.05.027 (2016).

13 Nowaczyk, M. J. *et al.* A novel multisystem disease associated with recessive mutations in the tyrosyl-tRNA synthetase (YARS) gene. *Am J Med Genet A* **173**, 126-134, doi:10.1002/ajmg.a.37973 (2017).

14 Fuchs, S. A. *et al.* Aminoacyl-tRNA synthetase deficiencies in search of common themes. *Genet Med* **21**, 319-330, doi:10.1038/s41436-018-0048-y (2019).

15 Casey, J. P. *et al.* Clinical and genetic characterisation of infantile liver failure syndrome type 1, due to recessive mutations in LARS. *J Inherit Metab Dis* **38**, 1085-1092, doi:10.1007/s10545-015-9849-1 (2015).

16 Lenz, D. *et al.* Genotypic diversity and phenotypic spectrum of infantile liver failure syndrome type 1 due to variants in LARS1. *Genet Med*, doi:10.1038/s41436-020-0904-4 (2020).

17 Wang, Z., Song, J., Luo, L. & Ma, J. Loss of Leucyl-tRNA synthetase b leads to ILFS1-like symptoms in zebrafish. *Biochem Biophys Res Commun* **505**, 378-384, doi:10.1016/j.bbrc.2018.09.133 (2018).

18 Hruscha, A. *et al.* Efficient CRISPR/Cas9 genome editing with low off-target effects in zebrafish. *Development* **140**, 4982-4987, doi:10.1242/dev.099085 (2013).

19 Hwang, W. Y. *et al.* Efficient genome editing in zebrafish using a CRISPR-Cas system. *Nat Biotechnol* **31**, 227-229, doi:10.1038/nbt.2501 (2013).

20 Peroutka, C. *et al.* Severe Neonatal Manifestations of Infantile Liver Failure Syndrome Type 1 Caused by Cytosolic Leucine-tRNA Synthetase Deficiency. *JIMD Rep* **45**, 71-76, doi:10.1007/8904_2018_143 (2019).

21 Her, G. M., Chiang, C. C., Chen, W. Y. & Wu, J. L. In vivo studies of liver-type fatty acid binding protein (L-FABP) gene expression in liver of transgenic

zebrafish (Danio rerio). *FEBS Lett* **538**, 125-133, doi:10.1016/s0014-5793(03)00157-1 (2003).

22 Her, G. M., Yeh, Y. H. & Wu, J. L. 435-bp liver regulatory sequence in the liver fatty acid binding protein (L-FABP) gene is sufficient to modulate liver regional expression in transgenic zebrafish. *Dev Dyn* **227**, 347-356, doi:10.1002/dvdy.10324 (2003).

23 Liu, Y. & Levine, B. Autosis and autophagic cell death: the dark side of autophagy. *Cell Death Differ* **22**, 367-376, doi:10.1038/cdd.2014.143 (2015).

24 Bai, H., Inoue, J., Kawano, T. & Inazawa, J. A transcriptional variant of the LC3A gene is involved in autophagy and frequently inactivated in human cancers. *Oncogene* **31**, 4397-4408, doi:10.1038/onc.2011.613 (2012).

25 Matsushita, M. *et al.* Structure of Atg5.Atg16, a complex essential for autophagy. *J Biol Chem* **282**, 6763-6772, doi:10.1074/jbc.M609876200 (2007).

26 Hu, Z., Zhang, J. & Zhang, Q. Expression pattern and functions of autophagy-related gene atg5 in zebrafish organogenesis. *Autophagy* **7**, 1514-1527, doi:10.4161/auto.7.12.18040 (2011).

27 Yamamoto, A. *et al.* Bafilomycin A1 prevents maturation of autophagic vacuoles by inhibiting fusion between autophagosomes and lysosomes in rat hepatoma cell line, H-4-II-E cells. *Cell Struct Funct* **23**, 33-42, doi:10.1247/csf.23.33 (1998).

28 Naito, T., Kuma, A. & Mizushima, N. Differential contribution of insulin and amino acids to the mTORC1-autophagy pathway in the liver and muscle. *J Biol Chem* **288**, 21074-21081, doi:10.1074/jbc.M113.456228 (2013).

29 Sang, Z., Zhang, P., Wei, Y. & Dong, S. miR-214-3p Attenuates Sepsis-Induced Myocardial Dysfunction in Mice by Inhibiting Autophagy through PTEN/AKT/mTOR Pathway. *Biomed Res Int* **2020**, 1409038, doi:10.1155/2020/1409038 (2020).

30 Pickrell, A. M. & Youle, R. J. The roles of PINK1, parkin, and mitochondrial fidelity in Parkinson's disease. *Neuron* **85**, 257-273, doi:10.1016/j.neuron.2014.12.007 (2015).

31 Long, Z. *et al.* Dynamic changes of autophagic flux induced by Abeta in the brain of postmortem Alzheimer's disease patients, animal models and cell models. *Aging (Albany NY)* **12**, 10912-10930, doi:10.18632/aging.103305 (2020).

32 Kostrikis, L. G. *et al.* Genetic analysis of human immunodeficiency virus type 1 strains from patients in Cyprus: identification of a new subtype designated subtype I. *J Virol* **69**, 6122-6130 (1995).

33 Ota, S. *et al.* Efficient identification of TALEN-mediated genome modifications

using heteroduplex mobility assays. *Genes Cells* **18**, 450-458, doi:10.1111/gtc.12050 (2013).

34 Kwan, K. M. *et al.* The Tol2kit: a multisite gateway-based construction kit for Tol2 transposon transgenesis constructs. *Dev Dyn* **236**, 3088-3099, doi:10.1002/dvdy.21343 (2007).

35 Hartley, J. L., Temple, G. F. & Brasch, M. A. DNA cloning using in vitro site-specific recombination. *Genome Res* **10**, 1788-1795, doi:10.1101/gr.143000 (2000).

36 Miyahara, H. *et al.* Suppressed expression of autophagosomal protein LC3 in cortical tubers of tuberous sclerosis complex. *Brain Pathol* **23**, 254-262, doi:10.1111/j.1750-3639.2012.00634.x (2013).

37 Miyahara, H. *et al.* Neuronal differentiation associated with Gli3 expression predicts favorable outcome for patients with medulloblastoma. *Neuropathology* **34**, 1-10, doi:10.1111/neup.12052 (2014).

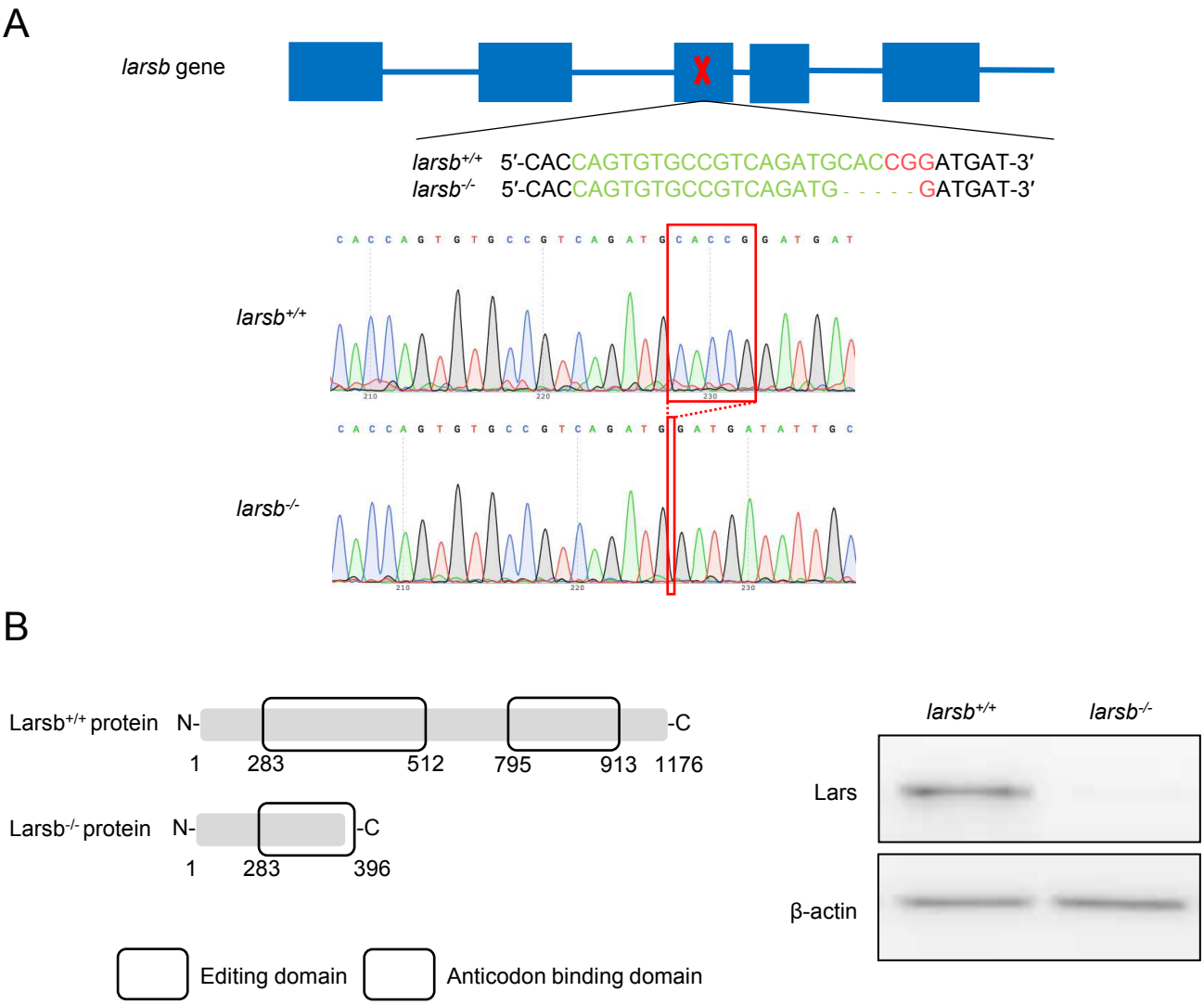
A
larsb gene
larsb+/+ 5′-CACCAGTGTGCCGTCAGATGCACCGGATGAT-3′
larsb-/- 5′-CACCAGTGTGCCGTCAGATG - - - - - GATGAT-3′
larsb+/+
larsb-/-
B
Larsb+/+ protein N- -C
1 283 512 795 913 1176
Larsb-/- protein N- -C
1 283 396
Editing domain
Anticodon binding domain
larsb+/+
larsb-/-
Lars
β-actin

Figure. 1

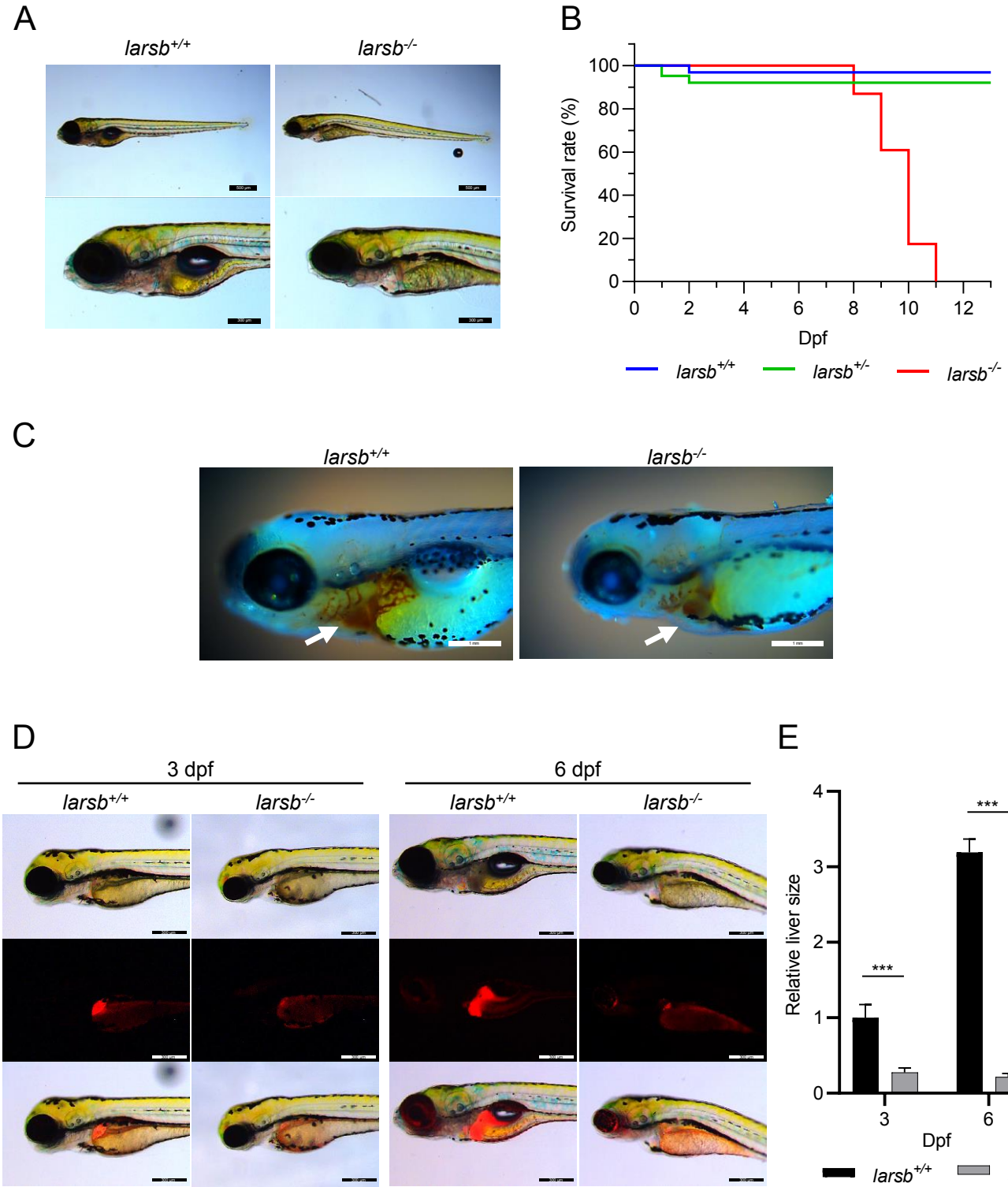
A
larsb+/+
larsb-/-
B
Survival rate (%)
100
80
60
40
20
0
0
2
4
6
8
10
12
Dpf
larsb+/+
larsb+/-
larsb-/-
C
larsb+/+
larsb-/-
D
3 dpf
6 dpf
larsb+/+
larsb-/-
larsb+/+
larsb-/-
E
Relative liver size
4
3
2
1
0
***
***
3
6
Dpf
larsb+/+
larsb-/-

Figure. 2

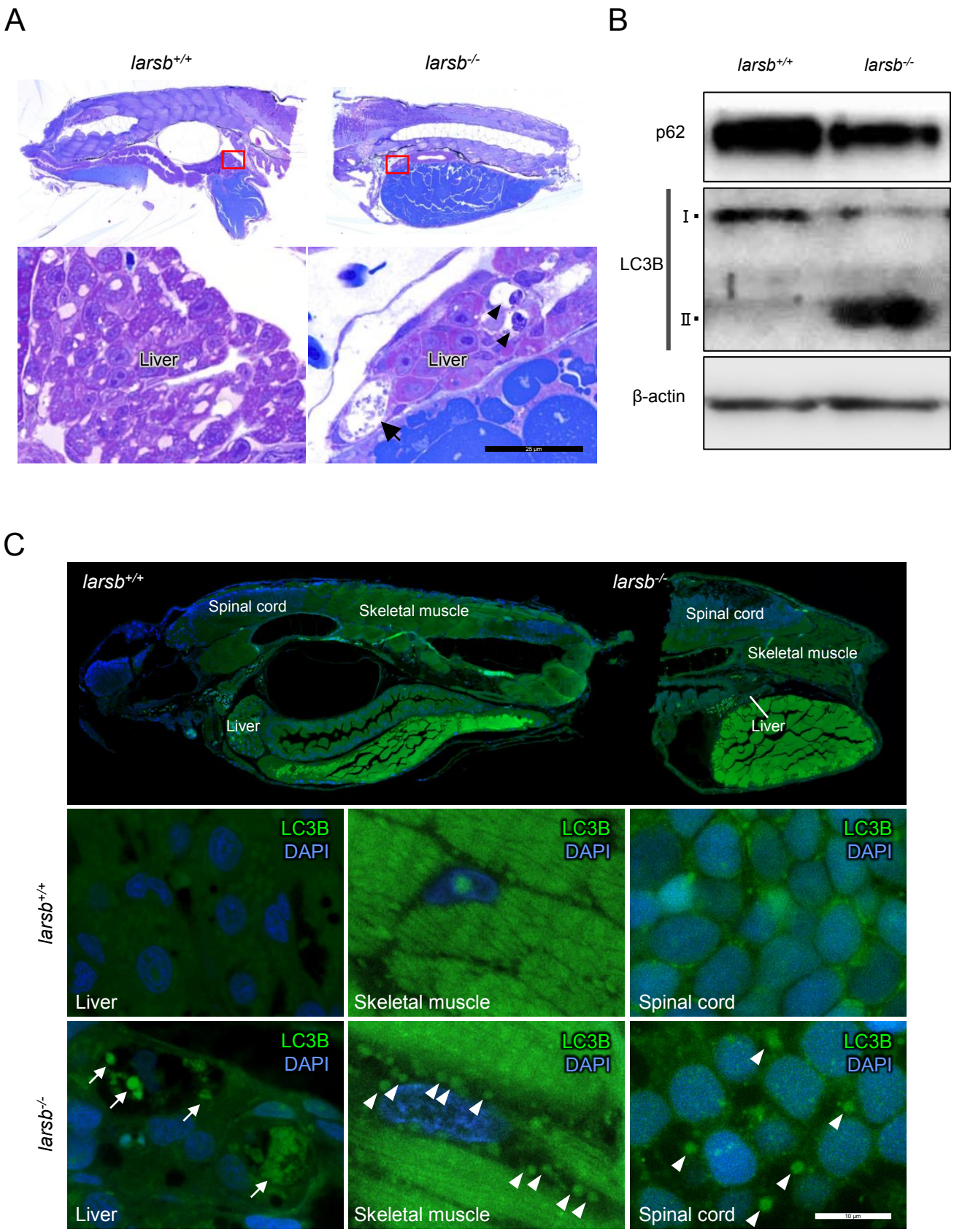
A
larsb+/+
larsb-/-
Liver
Liver
B
larsb+/+
larsb-/-
p62
LC3B
I
II
β-actin
C
larsb+/+
Spinal cord
Skeletal muscle
Liver
larsb-/-
Spinal cord
Skeletal muscle
Liver
larsb+/+
LC3B
DAPI
Liver
Skeletal muscle
Spinal cord
larsb-/-
Liver
Skeletal muscle
Spinal cord

Figure. 3

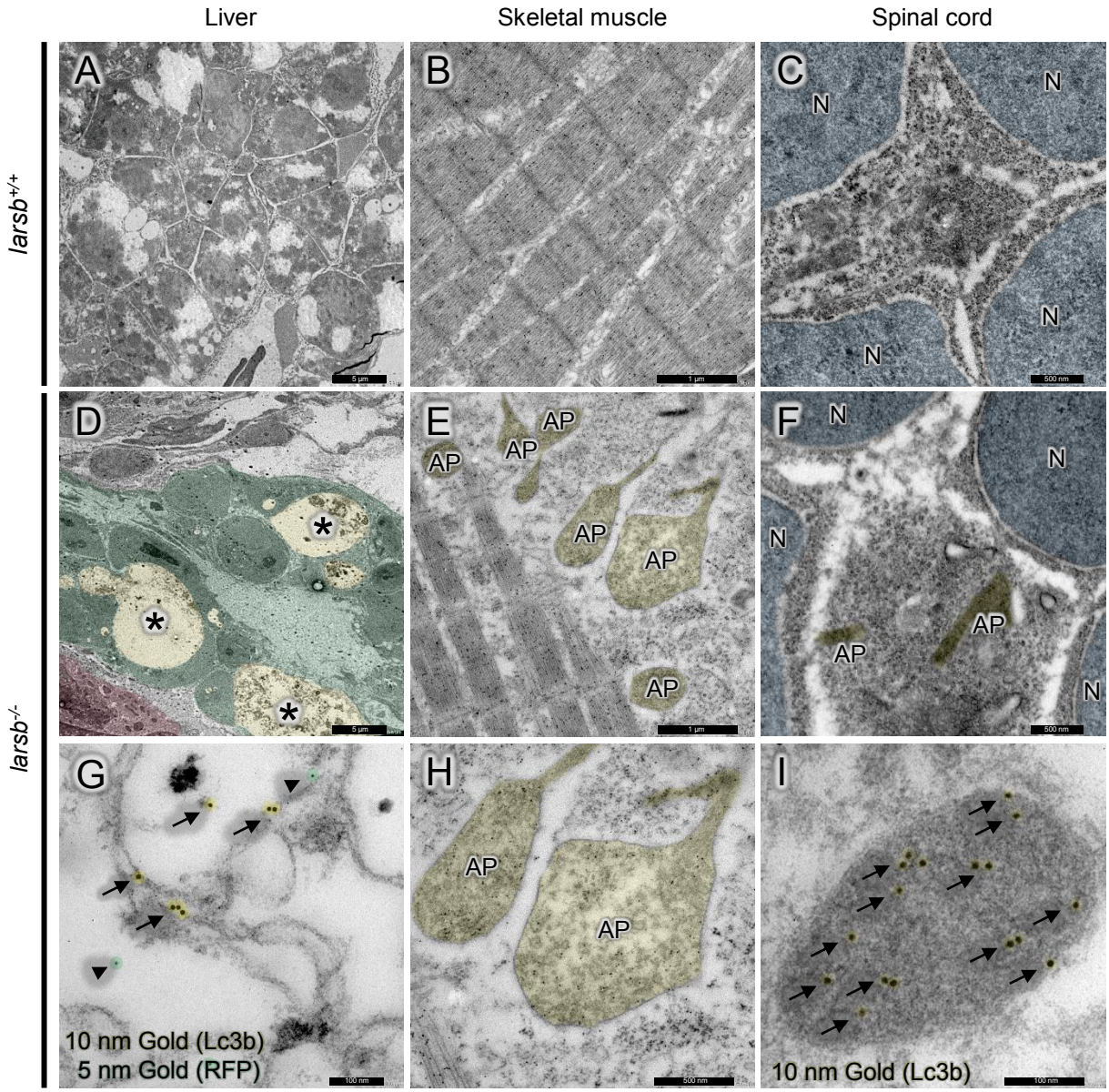
Liver
Skeletal muscle
Spinal cord
larsb+/+
larsb-/-
A
B
C
N
N
N
N
D
E
F
AP
AP
AP
AP
AP
AP
AP
AP
N
N
N
N
G
H
I
AP
AP
10 nm Gold (Lc3b)
5 nm Gold (RFP)
10 nm Gold (Lc3b)

Figure. 4

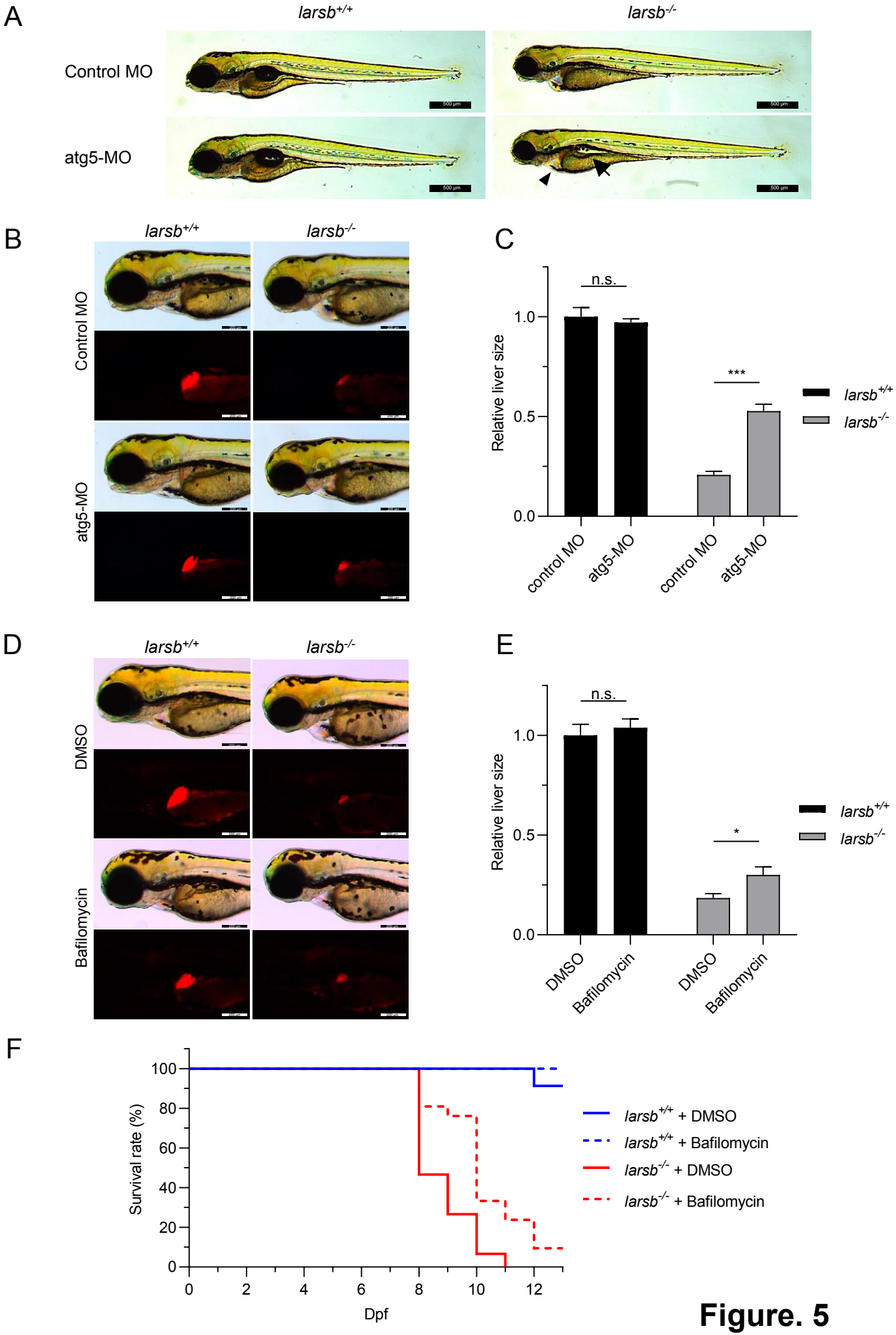
A
larsb+/+
larsb-/-
Control MO
atg5-MO
B
larsb+/+
larsb-/-
Control MO
atg5-MO
C
n.s.
***
Relative liver size
1.0
0.5
0.0
control MO
atg5-MO
control MO
atg5-MO
larsb+/+
larsb-/-
D
larsb+/+
larsb-/-
DMSO
Bafilomycin
E
n.s.
*
Relative liver size
1.0
0.5
0.0
DMSO
Bafilomycin
DMSO
Bafilomycin
larsb+/+
larsb-/-
F
Survival rate (%)
100
80
60
40
20
0
0
2
4
6
8
10
12
Dpf
larsb+/+ + DMSO
larsb+/+ + Bafilomycin
larsb-/- + DMSO
larsb-/- + Bafilomycin

Figure. 5

Figures

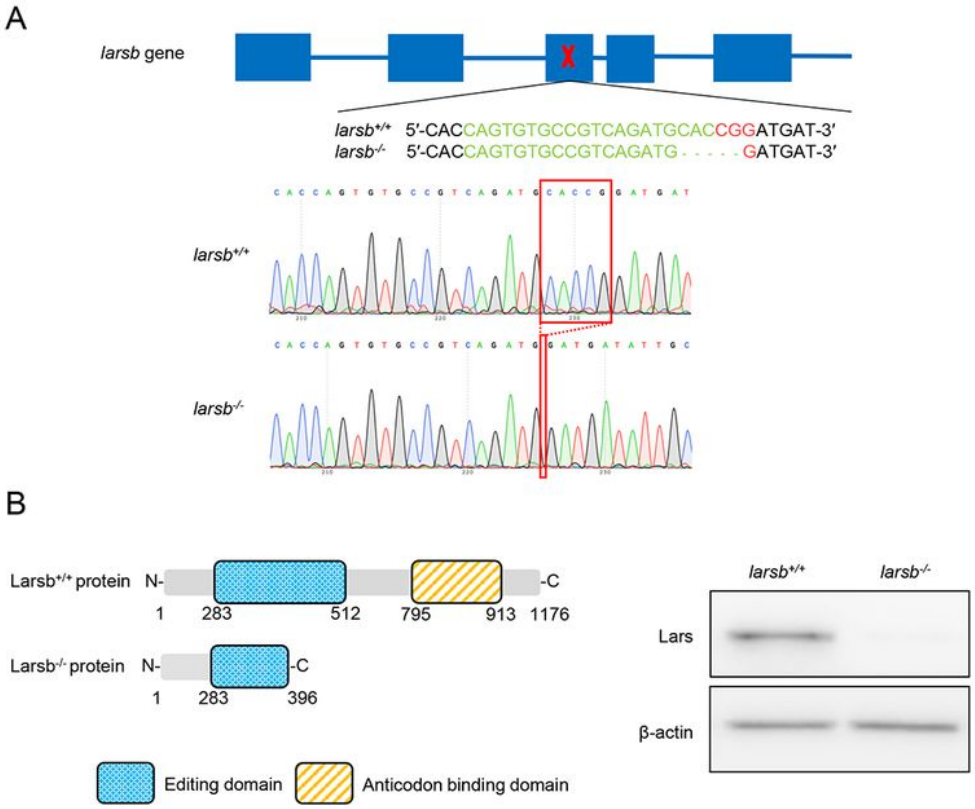

Figure. 1

Figure 1

Construction of larsb-knockout mutant zebrafish line. (A) Diagram showing the larsb genomic locus, CRISPR/Cas9 target site, and larsbknockout (larsb-/-) zebrafish mutant genotype. The sgRNA target sequence is displayed in green and the PAM region in red. In the genomic sequencing analysis

chromatograms, the deletion region in the mutant larsb-/- zebrafish is shown by the red box. (B) The Lars protein of larsb-/- zebrafish had a missing editing domain. Western blotting analysis of the Lars protein expression in larsb+/+ and larsb-/- zebrafish. β-actin levels served as the loading control. Lars: leucyl-tRNA synthetase.

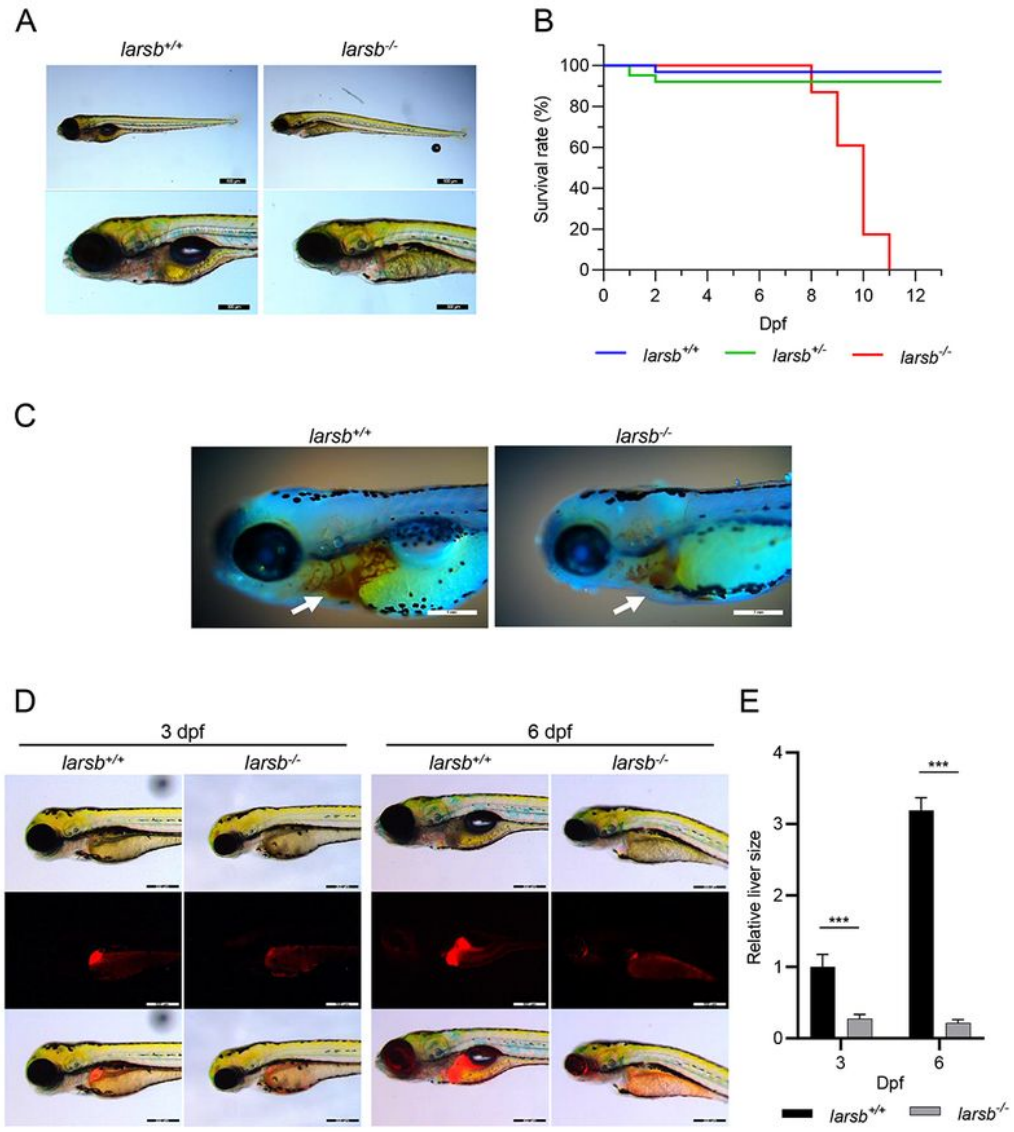

Figure. 2

Figure 2

Larsb-knockout larvae display severe developmental phenotype and liver abnormality with early lethality. (A) Bright field lateral views of larsb+/+ and larsb-/- embryos at 96 h post fertilization (hpf). Scale bar: 500 μm (top row) and 300 μm (bottom row). (B) Kaplan–Meier survival curve of larsb+/+ (n = 32), larsb+/- (n = 63), and larsb-/- (n = 23) larvae. (C) Lateral views of larsb+/+ and larsb-/- embryos containing haemoglobin-containing cells (white arrows) stained with o-dianisidine at 72 hpf. (D) Morphological abnormality at 3 dpf and 6 dpf in the livers of larsb-/- larvae under Tg[fabp10:mcherry] background. Scale bar: 300 μm. (E) Quantification of liver size in larsb-/- larvae under Tg[fabp10:mcherry] background (3 dpf and 6 dpf). n = 5 fish/group. Error bars indicate SEM. Student's t-test; ***P < 0.001. Lars: leucyl-tRNA synthetase; dpf: days post fertilization.

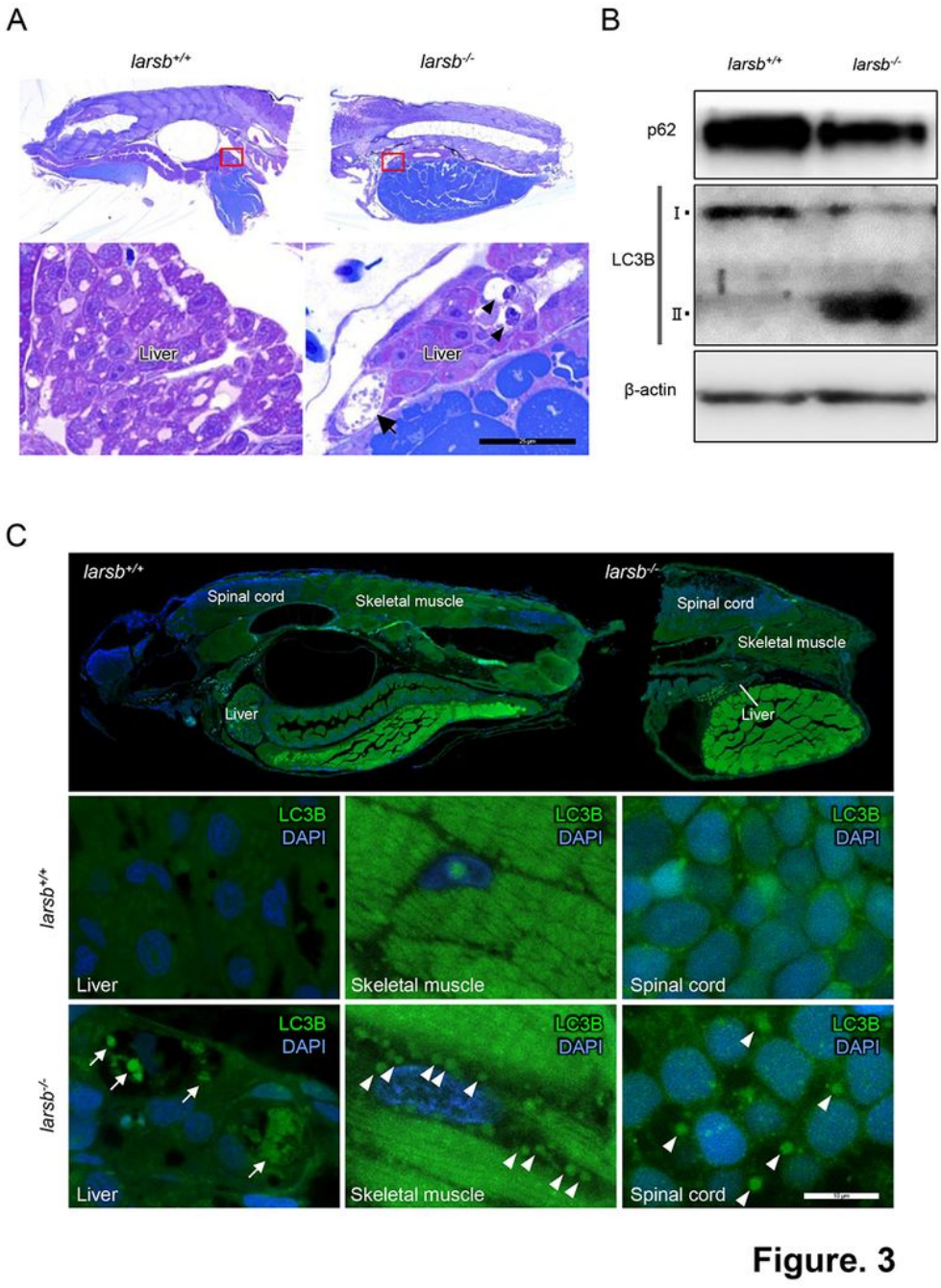

Figure. 3

Figure 3

Histopathology and fluorescent immunostaining of larsb-knockout larvae. (A) Lower magnification sagittal views (top row) and higher magnification views (bottom row) of larsb+/+ and larsb-/- larvae. Huge vacuolations, which seemed to disappear in the cytoplasm, were seen in the livers of larsb-/- larvae (black arrows), and some large vacuolations included a bare nucleus (black arrowheads). Scale bar: 25 μm. (B) Western blotting analysis of p62 and LC3B protein expression in larsb+/+ and larsb-/- larvae. β-

actin levels served as the loading control. (C) Lower magnification sagittal views of larsb+/+ and larsb-/- larvae (top row). Fluorescent immunostaining against LC3B (green) and DAPI (blue) of the livers, skeletal muscles, and spinal cords of larsb+/+ and larsb-/- larvae. Livers of larsb-/- larvae had large vacuoles, including floating nuclei and various sized dots with LC3B immunoreactivity (white arrows). Skeletal muscles and spinal cords of larsb-/- larvae had many dots with LC3B immunoreactivity (white arrowheads). Scale bar: 10 μm. Lars: leucyl-tRNA synthetase; LC3B: microtubule-associated protein 1A/1Blight chain 3; DAPI: 4',6-diamidino-2-phenylindole.

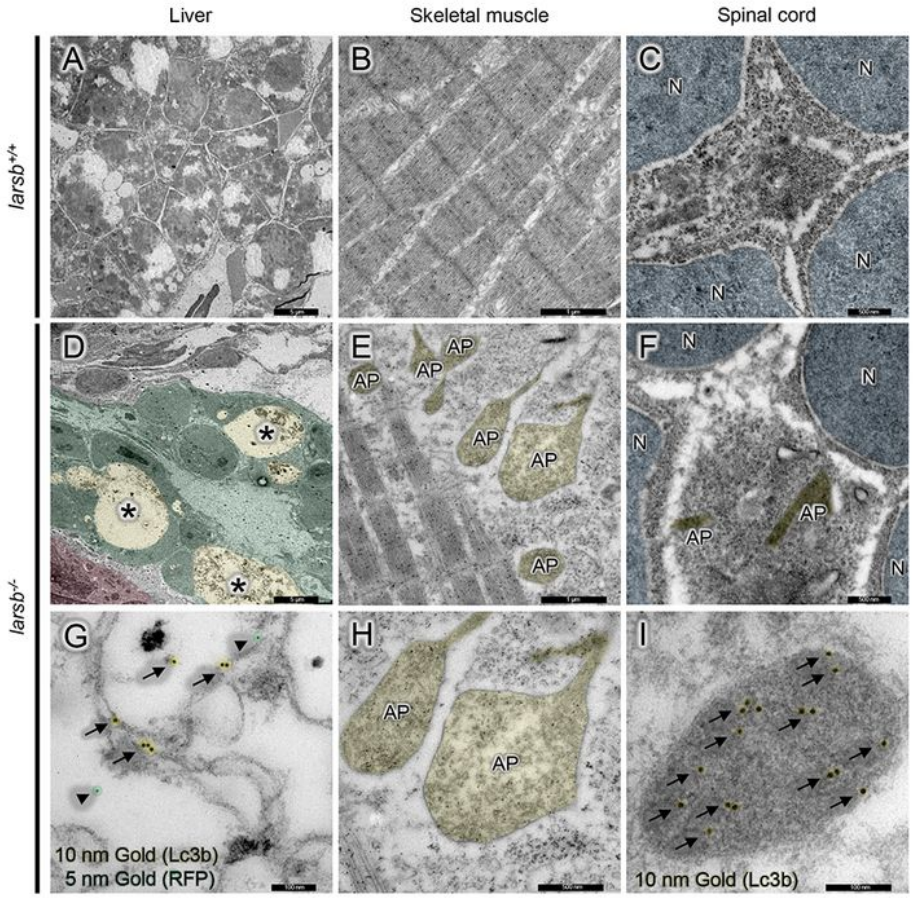

Figure. 4

Figure 4

Immunoelectron microscopy of larsb-knockout larvae. (A-C) Immunoelectron microscopy of the liver, skeletal muscle, and spinal cord of larsb+/+ larva. (D-I) Immunoelectron microscopy of the liver, skeletal muscle, and spinal cord of larsb-/- larva. The bottom row shows higher magnification images (G-I). Large vacuoles in the livers of larsb-/- larvae (asterisks) were composed of numerous irregular membranous structures, which showed immunoreactivity against both Lc3b (black arrows) and RFP (black arrowheads) (D and G). Scale bar: 5.0 μm for A and D; 1.0 μm for B and E; 500 nm for C, F, and H; 100 nm for G and I. AP: autophagosome, N: nucleus; Lars: leucyl-tRNA synthetase; Lc3b: microtubule-associated protein 1A/1B-light chain 3; RFP: red fluorescent protein.

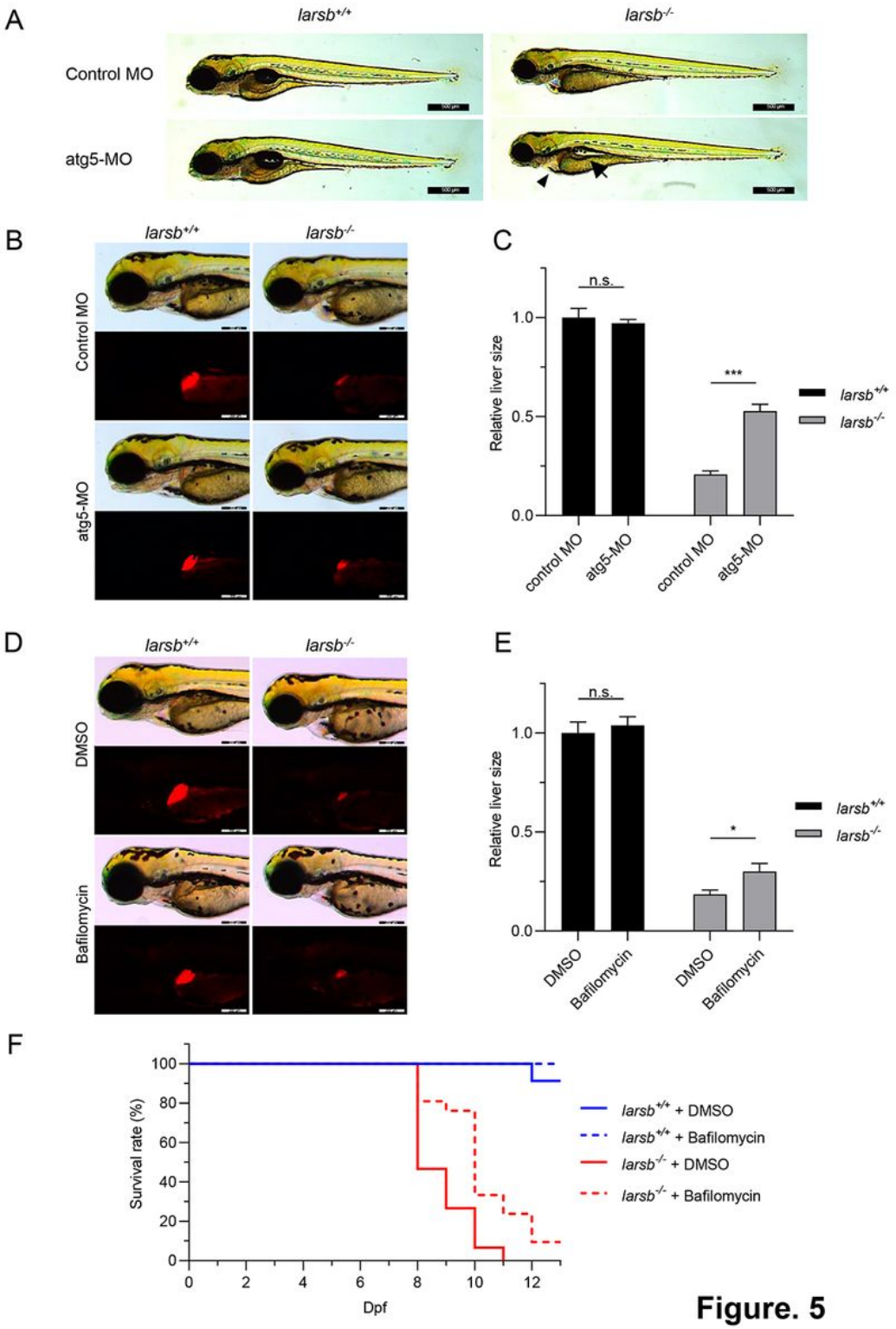

Figure. 5

Figure 5

Inhibition of autophagy prevents abnormal development and improves survival in larsb-knockout larvae. (A) Morphology of larsb+/+ and larsb-/- embryos injected with either control MO or atg5-MO (72 h post fertilization (hpf)). Scale bars: 500 μm. (B) Morphological abnormality at 72 hpf in the livers of larsb-/- larvae under Tg[fabp10:mcherry] background injected with either control MO or atg5-MO. Scale bars: 200 μm. (C) Quantification of liver size in larsb-/- larvae under Tg[fabp10:mcherry] background (72 hpf); n = 4

fish/group. Error bars indicate SEM. Student's t-test; ***P < 0.001. (D) Morphological abnormality at 72 hpf in the livers of larsb-/- larvae under Tg[fabp10:mcherry] background treated with DMSO or bafilomycin. Scale bars: 200 μm. (E) Quantification of liver size in larsb-/- larvae under Tg[fabp10:mcherry] background (72 hpf); n = 10 fish/group. Error bars indicate SEM. Student's t-test; *P < 0.05. (F) Kaplan–Meier survival curve of larsb+/+ (n = 23) and larsb-/- (n = 15) larvae treated with DMSO, and larsb+/+ (n = 11) and larsb-/- larvae (n = 21) treated with bafilomycin. Lars: leucyl-tRNA synthetase; MO: morpholino; n.s.: non-significant; DMSO: dimethyl sulfoxide; Dpf: days post fertilization.

Supplementary Files

This is a list of supplementary files associated with this preprint. Click to download.

- larsbsupfig.pdf